*Research Article*

# Binder-Loaded Amorphous Nanometer Calcium Phosphate in Preventing Enamel Demineralization in Orthodontic Patients

**Juan Gao [ID],[1] Ni Dang,[2] Qian Zhang,[3] Ying Liang,[1] Xue Wei,[1] and Anxiu Xu[1]**

[1]*Department of Orthodontics, Guiyang Hospital of Stomatology, Guiyang, 550002 Guizhou, China*
[2]*Department of Stomatology, Xi'an Hospital of Traditional Chinese Medicine, Xi'an, 710000 Shaanxi, China*
[3]*Temporomandibular Joint Expert Clinic, Guiyang Hospital of Stomatology, Guiyang, 550002 Guizhou, China*

Correspondence should be addressed to Juan Gao; 1253848776@qq.com

With the popularization of oral health knowledge, people have gradually realized the importance of orthodontic treatment in oral health, so the number of patients undergoing orthodontic treatment has increased significantly. To improve the effect of orthodontic treatment, this article mainly studied the application of adhesives loaded with amorphous nanocalcium phosphate in the prevention of enamel demineralization in orthodontic patients. In the experiment, we used spray-drying technology to synthesize NACP. The collected dry particles were dispersed with absolute ethanol, sonicated for 10 minutes, dropped on a 200 ordinary carbon support film, and then dried and observed with a transmission electron microscope (TEM). Prevention of enamel demineralization in orthodontic patients was by adhesive-loaded amorphous nanocalcium phosphate. In this experiment, the membrane dialysis method was used to release the drug-loaded nanoparticles. The MH-5 microhardness tester was used to randomly select 3 positions on the buccal area of the enamel surface to measure the microhardness. After measuring the microhardness of each point, take the average of the readings of the 3 positions. Before and after the experiment, the difference of the enamel surface microhardness before and after the experiment was statistically analyzed. Before the scanning electron microscope observation, to avoid contamination of the window area of the enamel surface, which will cause interference with the scanning electron microscope observation, we use acetone to remove the acid-resistant nail polish coated on the enamel surface. Clean the attachments on the surface of the teeth first, then fix, dehydrate, and dry. When the release time reaches 52 h, the cumulative release rates of Cur in pH 5.4 and pH 7.4 buffers are 85.84 and 64.68%, respectively. The results show that by adjusting the concentration of PAA, it is possible to configure a mineralized liquid that can not only use the fluidity of NACP to penetrate into the collagen fibers but also transform into HAP within a suitable time, to achieve the purpose of repairing demineralized dentin.

## 1. Introduction

In recent years, inorganic nanoparticles have attracted much attention due to their unique materials and size dependence. In addition to its good stability, easy control of morphology, and size, it also has optical, magnetic, and other physical properties and has a wide range of applications in drug delivery and tumor imaging. The chemotherapeutic drugs are loaded on the surface and pore structure of inorganic nanoparticles through physical, chemical action, or surface functional groups, and the drugs are transported into the organism through the cell membrane to achieve the therapeutic effect. Calcium phos-

phate is a typical inorganic nanoparticle, which has good biocompatibility and will not cause rejection in the organism, so it has obvious advantages in drug delivery, bioceramics, and bone repair. In organisms, ACP has better osteoconductivity and biodegradability than HAP and TCP, and some of its properties can be adjusted by changing its components. Amorphous calcium phosphate (ACP) is a general term for short-range ordered and long-range disordered calcium phosphates. ACP can be classified as having a variable chemical composition (the Ca/P ratio can vary from 1.0 to 2.0), a class of calcium phosphate salts with similar chemical properties to glass. ACP is an amorphous intermediate phase of calcium

phosphate found during the synthesis of hydroxyapatite (HAP) under neutral or acidic conditions, so X-ray diffraction analysis shows amorphous features.

Among calcium phosphate materials, ACP exhibits better osteoconductivity and biodegradability and has been widely used in the demineralization and remineralization of tooth enamel, bone defect treatment, and drug carriers. However, ACP is a metastable phase, it is very easy to transform into a crystal form, and it has poor dispersion in solution and is easy to agglomerate, which seriously affects the application of ACP in organisms. CPP-ACR (casein phosphopolypeptide-amorphous calcium phosphate) can effectively prevent enamel demineralization and promote the remineralization of enamel demineralization that has occurred.

Jiang et al. prepared stable nanoamorphous calcium phosphate (NACP) with polyethylene glycol as a stabilizer to obtain nanosized amorphous adsorbents [1]. Feng et al. explored the effect of a novel bioabsorbable stent composed of PLLA and ACP nanoparticles on inflammation and calcification of surrounding tissue after stent implantation in porcine coronary arteries [2]. Zhang et al. performed 20 cycles of hypophosphite adsorption-desorption on the polymer-supported ferric iron nanocomposite HFO@201 [3].

When fluoride is used alone, remineralization mainly occurs on the surface of tooth enamel caries. Once fluoride ions contact calcium and phosphorus ions, fluorapatite will quickly form on the surface of the tooth, preventing mineral ions from continuing to enter the caries. The deep layer hinders the remineralization of the deep layer. When CPP and fluoride ions exist at the same time, the entire layer of enamel caries can be remineralized. CPP can prevent the rapid transformation of calcium phosphate stage, and the mineral components can diffuse in the form of ions. Below the surface of the carious lesion, an active gradient is formed, which promotes remineralization throughout the entire layer of enamel carious lesions. This in vitro remineralization model after enamel acid etching strongly illustrates that lysozyme can stabilize a higher concentration of calcium and phosphorus ions into an amorphous state. Under the degradation of sodium hypochlorite and the induction of glycine, it can promote the remineralization of early enamel caries.

## 2. Method and Experiment

### 2.1. Experimental Equipment and Materials.
The main instruments are incubator, microhardness tester, laboratory PH meter, bt25s electronic scale, anaerobic culture tank, 61MXW-80A vortex oscillator, GSP-9050MBE constant temperature water-proof incubator, complete automatic biochemical analyzer, scanning electron microscope, energy spectrum analyzer, etc. [4].

The main materials used in the experiment are dipotassium hydrogen phosphate, calcium chloride dihydrate, 4-hydroxyethylpiperazine, ethanesulfonic acid, 1% sodium hypochlorite rinse, 37% phosphoric acid gel, etc. [5].

### 2.2. Subjects.
100 patients were randomly selected from the fixed orthodontic patients, 50 males and 50 males, aged between 12 and 16 years old, with permanent teeth. All patients were treated with the standard square wire arch technique, and the average treatment period was 20 months, which was set as the observation group. The control group consisted of a random selection of 200 normal people aged 12-16 years without fixed correction, 100 men and women each.

*Inclusion criteria.* The experimental group had normal tooth morphology, well-developed enamel, and no hard tissue diseases such as enamel demineralization, fluorosis, and tetracycline. The control group was those with normal tooth morphology, no enamel development defects, and no enamel demineralization.

*Exclusion criteria.* The experimental group was unable to follow up on time and adhere to treatment, and the control group were tetracycline teeth, fluorosis teeth, and other enamel development defects [6].

### 2.3. Synthesis of Nanometer Amorphous Calcium Phosphate (NACP).
Spray-drying technology was used to synthesize NACP. 1.5125 g anhydrous acetic acid was added to 500 mL distilled water to prepare a spray solution. Then, 0.8 g calcium carbonate ($CaCO_3$) and 5.094 g anhydrous calcium hydrogen phosphate ($CaHPO_4$) were dissolved in acetic acid solution. Add distilled water to the solution until the total volume of the solution reaches 1 L. The concentration of acetic acid is 25 mmol/L. The solution is sprayed by a nozzle located in a spray chamber with hot air flow at 10 mL/min feed rate. The collected dry particles were dispersed with absolute ethanol, vibrated with ultrasonic for 10 minutes, dropped on a 200 ordinary carbon support films, and observed by transmission electron microscope (TEM) after drying. The powder specific bet (Brunauer-Emmet-Teller) specific surface area was analyzed using a physical/chemical adsorption analyzer [7]. The preparation of NACP nanoparticles is shown in Figure 1.

Amorphous calcium phosphate (ACP) is generally considered a transition phase in the formation of calcium phosphate in aqueous environments. Generally speaking, ACP may be the first phase in the precipitation and crystallization process of calcium phosphate solution, which can be obtained by the rapid mixing of calcium and phosphorus solutions. The chemical composition of ACP is not fixed and is often related to the calcium and phosphorus concentrations and pH values in the reaction solution. As for the structure of the ACP, there is no clear conclusion so far. The IR spectrum of ACP shows a broad absorption peak for phosphate radicals. XRD results show that the compound is amorphous Through electron microscopy, it can be observed that ACPs are generally round spheres with diameters between 20 and 200 nm. ACP appears to have the short-range structure of apatite, but due to the very small size of the crystals, it shows an amorphous phase on the XRD pattern. This conclusion has been confirmed by X-ray absorption spectroscopy.

Sodium cyclopentadienyl is a colorless solid, but the sample will appear pink due to oxidation. Solutions of sodium cyclopentadienyl in THF are commercially available. It can be prepared by treating cyclopentadiene with sodium. The reaction is usually carried out by heating sodium to a molten state in dicyclopentadiene. Previously common practice was to use "sodium wire" or "sodium sand," which was obtained
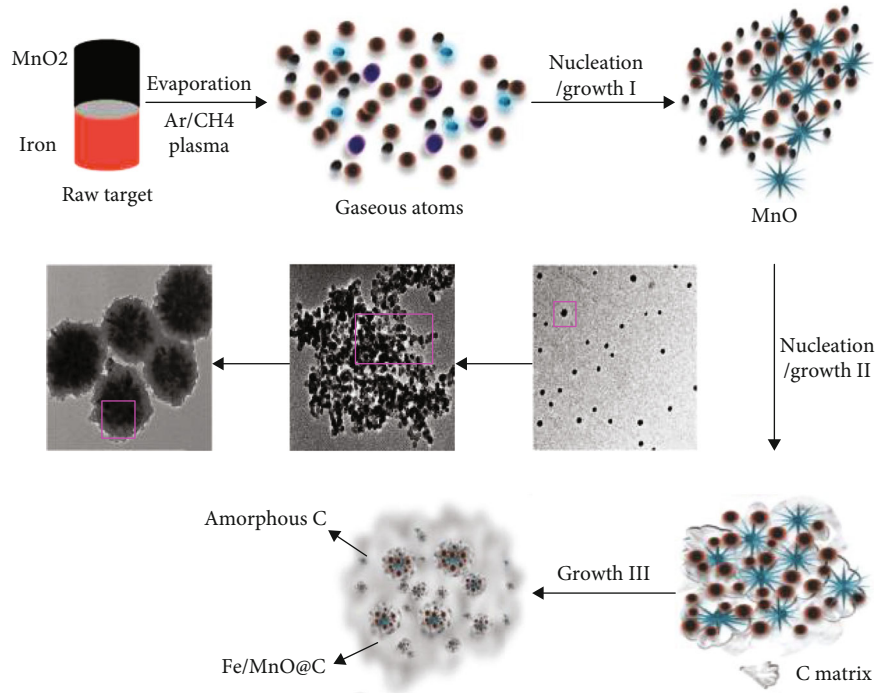
FIGURE 1: Preparation of NACP nanoparticles.

in the form of fine dispersion by melting and refluxing sodium in xylene with rapid stirring.

Define a binary comparison criterion [8]:

$$\tau(p; x, y) = \begin{cases} 1, & p(x) < p(y), \\ 0, & p(x) \geq p(y). \end{cases} \quad (1)$$

The formula is as follows [9]:

$$Z = \iint_w g(X)g^T(X)dX,$$
$$G(i,j) = \sqrt{G_x^2(i,j) + G_y^2(i,j)}, \quad (2)$$
$$\theta(i,j) = \arc\left(\frac{G_x(i,j)}{G_y(i,j)}\right).$$

When the image is blurred and the noise is small, the working state of the gradient operator is a satisfactory continuous image $f(x, y)$, and the position gradient $(x, y)$ can be expressed as a carrier [10]. If $G_x$ and $G_y$ are used to represent the gradient change of $f(x, y)$ along the $X$ and $Y$ directions, the gradient vector can be expressed as follows [11]:

$$f(x, y) = \begin{bmatrix} \dfrac{\partial f(x, y)}{\partial x} \\ \dfrac{\partial f(x, y)}{\partial y} \end{bmatrix}. \quad (3)$$

A transformation method based on the tangent function is as follows [12]:

$$D_o = \frac{D_M}{2}\left[1 + \frac{\tan\left(\alpha\pi(x/D_M - 1/2)\right)}{\tan\left(\alpha\pi/2\right)}\right]. \quad (4)$$

The specific steps of the BP neural network algorithm are as follows: each connection has a weight. If the $j$-node is in the exit layer or the hidden layer [12], the net input to the $j$-node $E_j$ is as follows:

$$E_j = \sum_i w_{ij}S_i + \theta_j. \quad (5)$$

Given the net input $E_j$ of node $j$, the output of $S_j$ of node $j$ is as follows [13]:

$$S_j = \frac{1}{\left(1 + e^{-I_j}\right)}. \quad (6)$$

As the burden and bias representing the prediction error of the network are continuously updated, the error propagates backwards [14]. For the node of the output layer $j$, the error $\mathrm{Err}_j$ calculation formula is as follows:

$$\mathrm{Err}_j = S_j(1 - S_j)(G_j - S_j). \quad (7)$$

Computing the error of $j$ nodes on the hidden layer requires a weighted sum of $j$-related node errors on the next layer [15]. The error of the hidden layer of the $j$ node is as follows:

$$\mathrm{Err}_j = S_j(1 - S_j)\sum_k \mathrm{Err}_k w_{kj}. \quad (8)$$

$w_{jk}$ is the connection weight from node $k$ to node $j$ in the next higher layer [16], and $\text{Err}_k$ then is the error of node $k$.

The propagated errors are reflected by updating the weights and biases [17, 18]. The formula for weight update is as follows, where $\Delta w_{ij}$ is $w_{ij}$ the weight change amount.

$$\Delta w_{ij} = (1)\text{Err}_j S_i,$$
$$w_{ij} = w_{ij} + \Delta w_{ij}. \tag{9}$$

The offset is updated by the following equation, where $\Delta \theta_j$ is $\theta_j$ the offset change.

$$\Delta \theta_j = (1)\text{Err}_j,$$
$$\theta_j = \theta_j + \Delta \theta_j. \tag{10}$$

*2.4. In Vitro Drug Release.* In this experiment, membrane dialysis was used to release the drug-loaded nanoparticles. First, put 5 mL Cur-ACP nanoparticles (2 mg/mL) in a pretreated dialysis bag with a molecular weight cut-off of 34 kDa, immerse the dialysis bag in a 100 mL beaker (protect from light), and place the beaker in a shaker (37°C, 70 rpm) [19, 20]. The in vitro drug release process is shown in Figure 2.

*2.5. Antioxidant In Vitro.* In this determination, 1 mL of samples with various concentrations (2, 4, 6, 8, and 10 μg/mL) was mixed with 2 mL of 0.1 mM DPPH solution [21]. After that, the mixed solution was kept at room temperature and protected from light for 30 minutes [22].

$$\text{Inhibition}(\%) = \frac{A_0 - A_1}{A_0} \times 100\%. \tag{11}$$

Among them, $A_0$ is the absorbance of the control group, and $A_1$ is the absorbance of the sample.

*2.6. Preparation of New Antibacterial Remineralization Functional Orthodontic Adhesive.* As shown in Table 1, the first new type of orthodontic adhesive was prepared by adding 5% by mass of MAE-DB to PEHB resin. MAE-DB and NACP with mass ratios of 5% and 40% were added to PEHB to prepare the second new type of orthodontic adhesive, referred to as PND. Adding more than 40% of NACP to the resin will affect the adhesive properties and mechanical properties of the resin, so the addition concentration of 40% is selected. The whole preparation process is carried out in a dark room, and the resin mixture is mixed evenly with a mixing knife, and the air bubbles are removed by vacuum. The adhesive is prepared within 0.5 h before each use, and the unused ones are discarded after the test and no longer used [23, 24].

Take 0.5 g of mussel shell powder in a 100 mL beaker, add 40 mL of propionic acid with a concentration of 5% to make it fully react, take the supernatant after centrifugation, dilute the obtained solution to 50 mL, and then dilute the concentration to 0.06 M 50 mL of phosphoric acid solution was added dropwise to the beaker. After the dropping was

completed, 0.6 mmol of sodium tripolyphosphate was added to the beaker. After 30 min of reaction, 6 g of urea was added. After stirring to fully dissolve the urea, the beaker was placed at 90°C. In a water bath, it was stirred for 3 min and then allowed to stand until precipitation appeared. The precipitate was centrifuged, washed twice with deionized water and twice with ethanol, and dried at 70°C for 24 h to obtain ACP white powder.

*2.7. Testing of Mechanical Properties of New Orthodontic Adhesives.* Transbond XT paste (TB), a commonly used orthodontic adhesive in clinical practice, was selected as a commercial control, and three adhesives (TB, PD, and PND) were used to make test pieces with a size of 25 mm × 2 mm × 2 mm. The surface was cured with LED light curing lamp (output light intensity is 1200 mW/cm$^2$) for 60 s. After fully curing, the specimen was placed in a constant temperature water bath at 37°C for 24 h. Each group has 5 test pieces. A three-point bending test was carried out on a computer-controlled universal testing machine with a span of 20 mm and a pressing speed of 1 mm/min, to test the flexural strength and elastic modulus of the material. The flexural strength is calculated by the following formula [25]:

$$S = 3P_{\max} \frac{L}{(2bh^2)}. \tag{12}$$

Among them, $P_{\max}$ is the breaking load, $L$ is the span, $b$ is the width of the specimen, and $h$ is the height of the specimen.

The modulus of elasticity is calculated by the following formula:

$$E = \left(\frac{P}{d}\right)\left[\frac{L^3}{(4bh^3)}\right]. \tag{13}$$

The load $P$ divided by the displacement $d$ is the slope of the load-displacement curve in the linear elastic region [26].

*2.8. Microhardness Measurement.* In this experiment, the MH-5 microhardness instrument was used to randomly select 3 positions on the buccal test area of the enamel surface to measure the microhardness. After measuring the microhardness of each point, the average of the readings of the 3 positions was taken. Use this method to calculate the final surface microhardness value of the tooth enamel. Nanohardness and elastic modulus are measured by a nanoindenter. The test uses a continuous hardness measurement method. The depth of pressure is 600 nm. The calculation formula of hardness and elastic modulus is as follows:

$$S = \beta\sqrt{\lambda}E_r h,$$
$$\frac{1}{E_r} = \frac{(1 - v_i^2)}{E_i} + \frac{(1 - v_s^2)}{E_s}. \tag{14}$$

In the formula, $S$ represents the contact hardness, $h$ represents the depth of pressure measurement, $E_r$ is the reduced
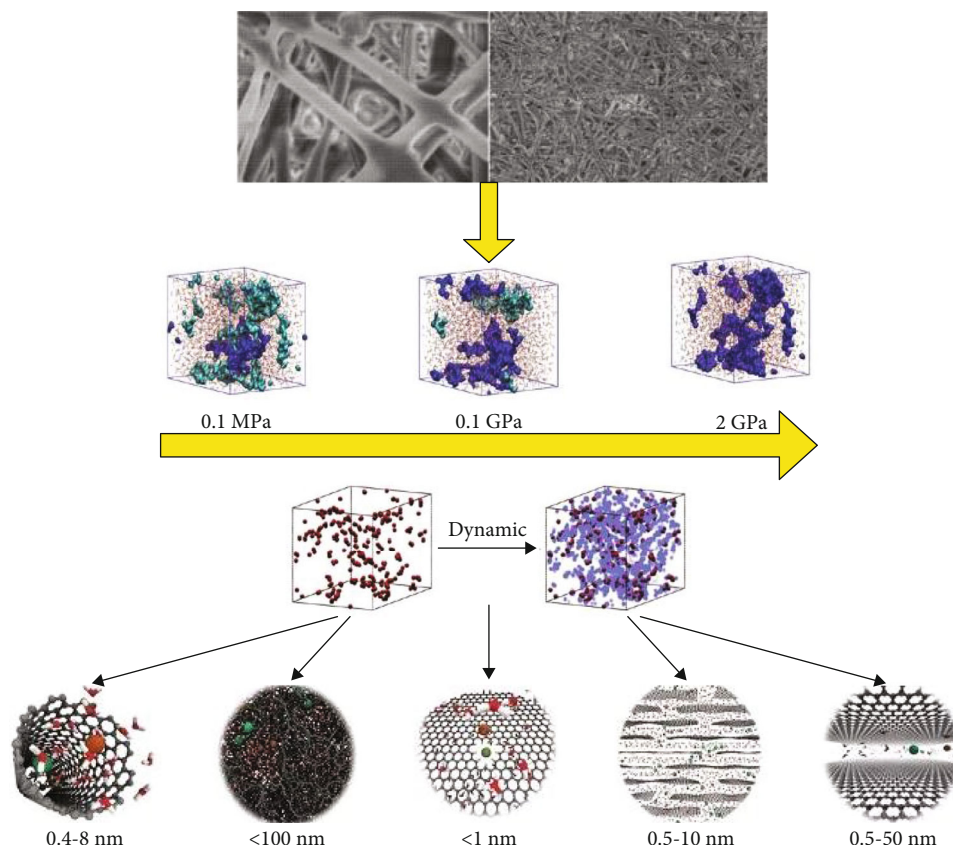
FIGURE 2: In vitro drug release process.

TABLE 1: Composition and mass fraction of two experimental adhesives.

| Glue | PEHB | MAE-DB | NACP |
|------|------|--------|------|
| PD | 95 | 5 | 0 |
| PND | 55 | 5 | 40 |

Young's modulus, and $E_i$ and $E_s$ are determined by the Young's modulus of the probe and the sample.

*2.9. Scanning Electron Microscope Surface Observation.* In this experiment, two samples were drawn from each group according to the random number table for scanning electron microscopy (JEOLJSM-6390LV) observation in the window area of the tongue and palate. Before the scanning electron microscope observation, to avoid contamination of the window area of the enamel surface, which will cause interference with the scanning electron microscope observation, we use acetone to remove the acid-resistant nail polish coated on the enamel surface. Clean the attachments on the surface of the teeth first, then fix, dehydrate, and dry. Because the surface of the tooth is not charged, its electrical conductivity is also relatively poor, so the charging effect and discharge effect will be caused when observing with a scanning electron microscope, which will affect the observation of the image of the enamel surface. Therefore, it is necessary to check the sample before observing the sample. The surface of the sample is sprayed with gold to increase the conductivity of the test surface of the sample. Finally, the samples are placed to the sample stage according to the original grouping order. When observing the image for collection, each experimental group can be distinguished according to the quadrant.

*2.10. Statistical Analysis.* All data were entered into the computer through EXCEL, and single-factor analysis was used to compare whether the enamel surface roughness values and microhardness values of each group were statistically different. The test standard was $P = 0.05$. The statistical results are completed by the SPSS13.0 statistical software.

## 3. Results

The comparative analysis of the labial surface pH of the upper and lower anterior teeth is shown in Figure 3. The results showed that no matter which group of patients, the pH was lower than that of the mandibular teeth, and the difference was statistically significant ($P < 0.05$).

Table 2 shows the comparison of the teeth between the anterior teeth of the same name. Table 3 shows the comparison of the labial pH of the teeth between the anterior teeth of the same name. It can be seen from the results that no matter the upper and lower jaws, there is no statistically significant difference in pH ($P > 0.05$).
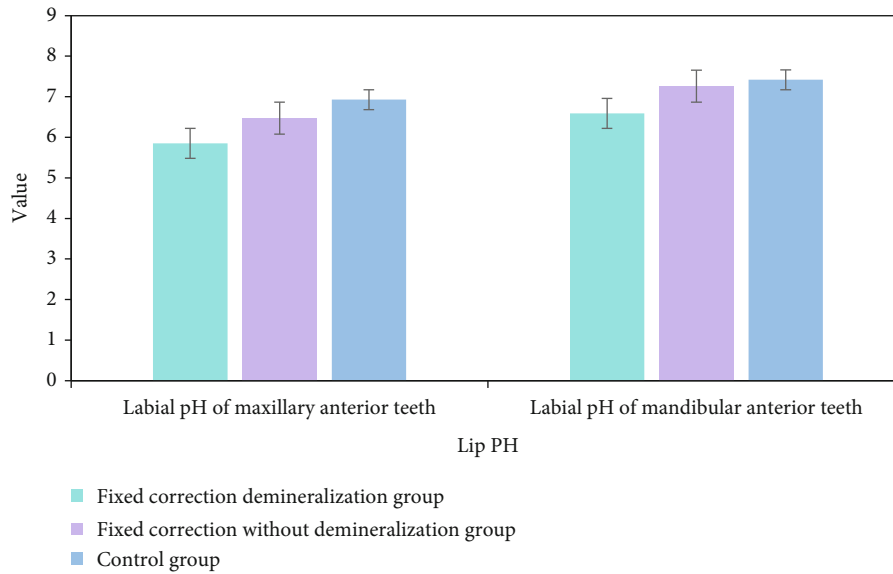
FIGURE 3: Comparative analysis of the labial pH of the upper and lower anterior teeth.

TABLE 2: Comparison of the labial pH between the left and right sides of the upper jaw with the same name anterior teeth.

| Tooth | Left | Right | $t$ | $P$ |
|-------|------|-------|-----|-----|
| I1 | $6.64 \pm 0.22$ | $6.71 \pm 0.15$ | 1.92 | >0.05 |
| I2 | $6.40 \pm 0.12$ | $6.46 \pm 0.20$ | 1.37 | >0.05 |
| C | $6.89 \pm 0.18$ | $6.91 \pm 0.17$ | 0.94 | >0.05 |

TABLE 3: Comparison of pH between the anterior teeth of the same name on the left and right sides of the mandible.

| Tooth | Left | Right | $t$ | $P$ |
|-------|------|-------|-----|-----|
| I1 | $7.29 \pm 0.28$ | $7.34 \pm 0.21$ | 1.29 | >0.05 |
| I2 | $7.33 \pm 0.23$ | $7.30 \pm 0.14$ | 0.87 | >0.05 |
| C | $7.07 \pm 0.16$ | $7.10 \pm 0.26$ | 0.73 | >0.05 |

Calcium phosphate remineralization method contributes to the prevention of enamel leukoplakia lesions and promotes remineralization of demineralized enamel. Dental resin materials containing calcium phosphate can release calcium and phosphorus ions, which become calcium and phosphorus ion reservoirs for plaque neutralization and tooth surface, preventing enamel demineralization and promoting remineralization.

The $N_2$ adsorption-desorption isotherm and BJH pore size distribution of NACP nanoparticles are shown in Figure 4. The sample shows an IV-type isotherm of H1 hysteresis loop, which is a typical mesoporous structure. From the measured data, it can be seen that the BET surface area of NACP nanoparticles is $41.414 \, \text{m}^2/\text{g}$, and the total pore volume and average pore diameter are about $0.165 \, 6 \text{cm}^3/\text{g}$ and $10.5 \, \text{nm}$, respectively.

Figure 5 shows the slow release process of NACP nanoparticles in vitro at 37°C and different pH. There was no sig-

nificant difference in the cumulative release of drugs in different pH buffers 5 h before release. However, as time increases, the drug release rate of Cur-ACP nanoparticles in pH 5.4 is faster than the release rate in pH 7.4. This is because NACP will gradually decompose in an acidic environment, thereby causing the loaded drug will be released slowly. When the release time reaches 52 h, the cumulative release rates of Cur in pH 5.4 and pH 7.4 buffers are 85.84 and 64.68%, respectively.

The quartiles of the proportion of Actinomycetes at different stages of treatment are shown in Figure 6. After wearing the fixed appliance, the proportion of some bacteria in the total flora also changed. Three kinds of bacteria (Streptococcus mutans, Lactobacillus, and Actinomycetes) accounted for the proportion of total bacteria. Kruskal-Wallis H rank-sum test analysis of multiple independent sample comparisons found that the proportions of Streptococcus mutans and Lactobacillus exist between group differences ($P < 0.05$). For the proportion of Actinomycetes in the total flora, there was no significant change among the groups ($P > 0.05$). Further use of pairwise comparison found that, compared with individuals who did not receive orthodontic treatment, the fixed appliance worn for less than 1 year, 1-2 years, and more than 2 years showed Streptococcus mutans and mutant in the local plaque of the tooth surface. The proportion of Lactobacillus in the total flora was significantly increased ($P < 0.05$), but the Kruskal-Wallis H rank-sum test analysis of multiple independent sample comparisons found that the proportion of Streptococcus mutans and Lactobacillus in the flora increases but does not occur continuously with the extension of the treatment time (the proportion of Streptococcus mutans and Lactobacillus in the partial plaque with the tooth surface after the fixed appliance is worn for less than 1 year, 1-2 years, and more than 2 years. The difference in proportion is not significant, $P > 0.05$).

The surface roughness of the seven different samples is shown in Figure 7. In the first month of the experiment, the
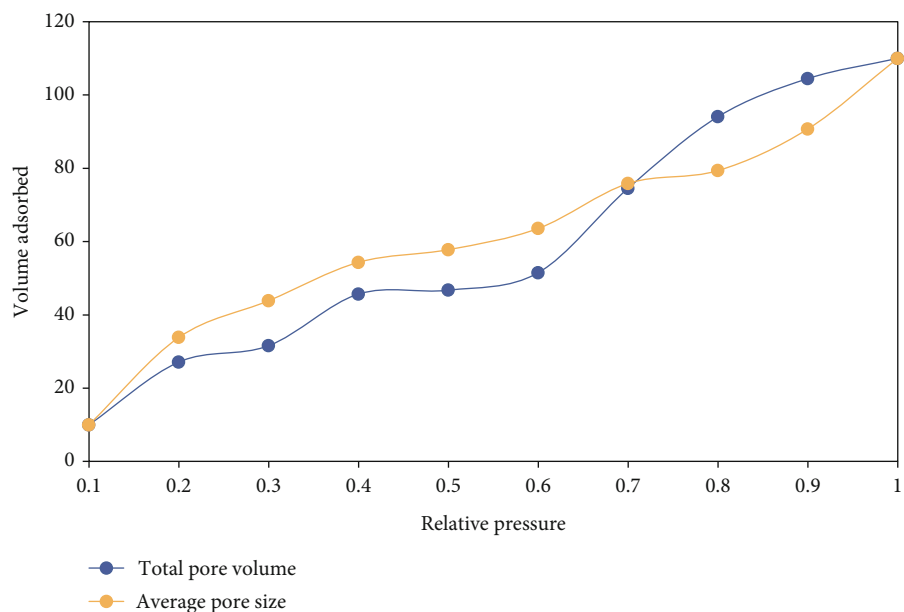
FIGURE 4: $N^2$ adsorption-desorption isotherm and BJH pore size distribution of NACP nanoparticles.
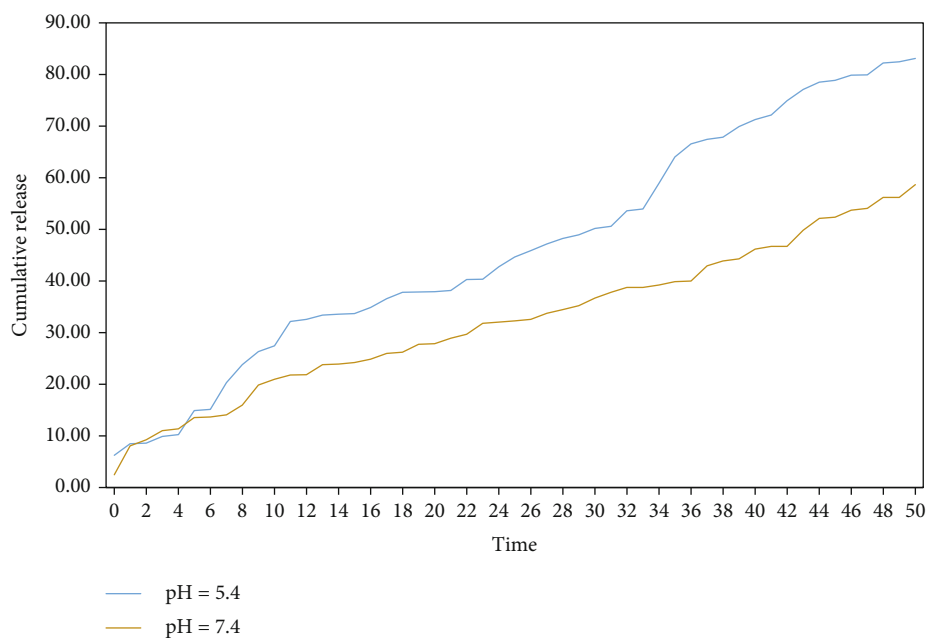


FIGURE 5: The slow drug release process of NACP nanoparticles in vitro at 37°C and different pH.

enamel surface roughness of the D group was significantly lower; two and three months of the experiment, the enamel surface roughness of each treatment group was significantly reduced. Compared with group G, the difference was significant ($P < 0.05$), the enamel surface roughness of group B was significantly lower than that of other groups ($P < 0.05$), and group C was significant compared with group D, group E, and group F difference. It can be seen that different influencing factors will have various effects on the surface roughness of different samples.

The scanning electron microscope situation is shown in Figure 8. In a dry environment, after the treatment of 37% phosphoric acid and GC treatment agent, the enamel cracks or enamel peeling of the GC adhesive group after two unloadings all showed different degrees of enamel cracking or enamel peeling, especially the second unloading was more prominent. In the area covered by the enamel adhesive, there are residual resin protrusions embedded in the micropores of the enamel after removing the brackets, and the bonding is tight, and the bonding surface has no obvious cracks.
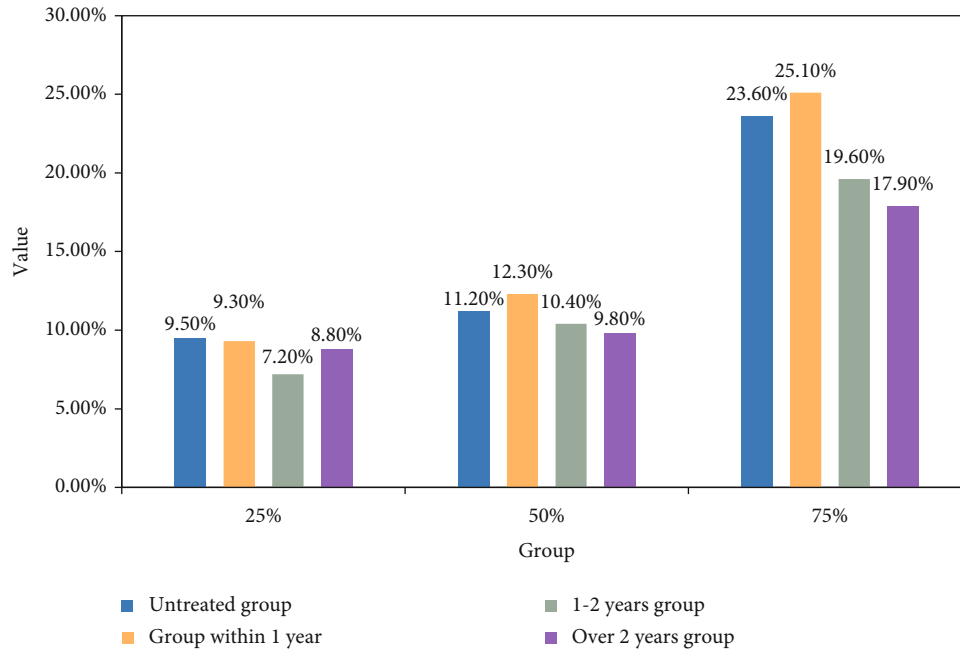
FIGURE 6: Quartiles of the proportion of Actinomycetes at different stages of correction.
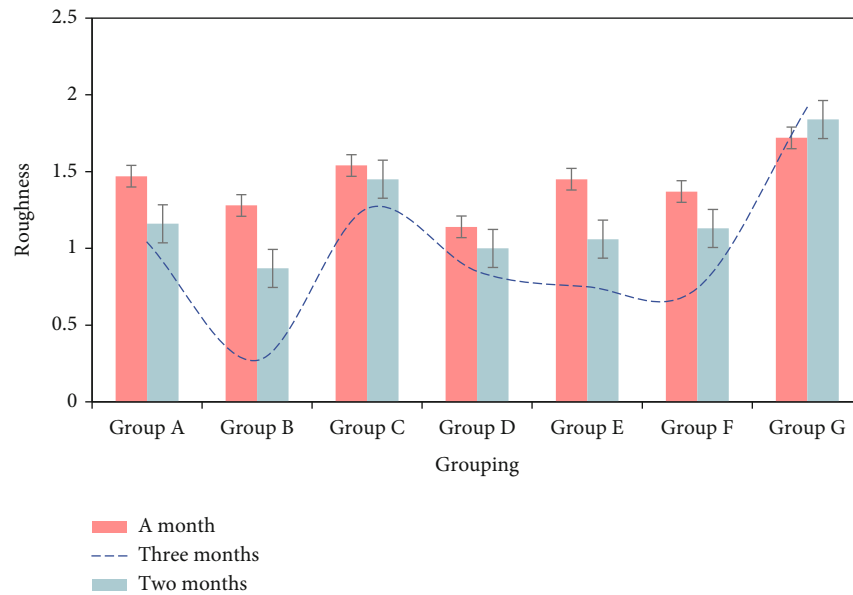


FIGURE 7: The surface roughness of seven different samples.

According to the analysis of the bonding process, these protrusions are mainly caused by no fillers. The liquid component of the enamel adhesive with good penetration and physical bonding properties is formed. This protrusion is considered beneficial to tooth health and still has an anticaries effect and does not need to be removed. Moreover, its anticaries effect compensates for the side effects caused by the improved bonding method to expand the acid etched area.

The comparison of the demineralization rates is shown in Table 4. Comparison of enamel demineralization rates

between groups A, B, and C is as follows: group B and group A are different in demineralization rate, group A is higher than group B ($\chi^2 = 19.227$, $P \leq 0.01$); group C is demineralized compared with group A. The rate is different in group A than in group C ($\chi^2 = 21.892$, $P \leq 0.01$); there is no difference in demineralization rate between group B and group C ($\chi^2 = 0.053$, $P = 0.818$). The new composite material based on the binder-loaded amorphous nanocalcium phosphate can effectively seal the open dentinal tubules, and its effect has a certain resistance to abrasion and acid, which provides
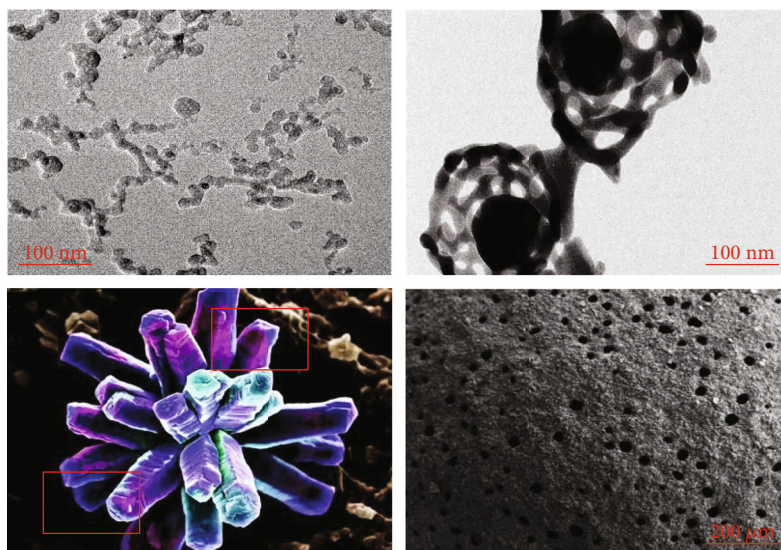
FIGURE 8: Scanning electron microscope situation.

TABLE 4: Comparison of the demineralization rate of the three groups A, B, and C.

| | Demineralization rate | $\chi^2$ value | $P$ value |
|---|---|---|---|
| Group A and group B | | | |
| Group A | 26.41 | 19.227 | ≤0.01 |
| Group B | 14.35 | | |
| Group A and group C | | | |
| Group A | 26.41 | 21.892 | ≤0.01 |
| Group C | 13.82 | | |
| Group B and group C | | | |
| Group B | 14.35 | 0.053 | 0.818 |
| Group C | 13.82 | | |

a new experimental basis for the clinical treatment of dentin hypersensitivity.

The averages of the three groups of EDI indexes A, B, and C are shown in Figure 9. It can be seen from the figure that the average of the EDI index of the group A is the highest. Comparison between group B and group A is as follows: $t = 2.929$, $P = 0.008$, group A is higher than group B, which is statistically significant; comparison between group C and group A is as follows: $t = 2.911$, $P = 0.008$, group A is higher than group C, and there is statistical significance; comparison between group B and group C is as follows: $t = 0.340$, $P = 0.737$, and there is no statistical significance.

The comparison of the numbers and proportions of the two groups of Streptococcus mutans and Actinomycetes is shown in Table 5. The number of Streptococcus mutans in the demineralization group was significantly increased compared with the nondemineralization group.

## 4. Discussion

The crystalline phase transition of ACP is an autocatalytic process, and its crystallization curve is s-shaped. Phase transition is the process in which a substance changes from one phase to another, so the crystallization process is a phase transition process. There are many factors that affect the phase transition of ACP, mainly including the pH value of the solution, the temperature of the system, and the addition of foreign ions or molecules. Under alkaline conditions, ACP finally phases into hydroxyapatite in aqueous solution, and the phase transition rate is very slow (pH = 9.00). The increase in acidity increases the speed of amorphous intersecting. At pH = 3.4, the amorphous phase only exists for a few minutes, but the phase becomes calcium-deficient hydroxyapatite (DCPD) instead of apatite, and ACP evolves to calcium-deficient under physiological pH conditions. And phosphate hydrolyzed apatite. Temperature has a great influence on the phase change of ACP. It takes about three days for the phase change at 10°C, two hours at 25°C, and complete phase change within 30 minutes when it rises to 37°C. The influence of foreign ions and molecules on the phase transition of ACP is also essential. In fact, organisms use the interaction of biological macromolecules with calcium ions and phosphate ions to control the amorphous as the precursor of biomineralization.

The change in the gloss of the tooth surface is one of the manifestations of demineralization. It will become caries if it develops further without treatment. Generally, tooth enamel demineralization can be divided into two forms, namely, surface demineralization and subsurface demineralization. After the remineralization of early enamel caries, mineral salts can stay in part of the enamel that has been demineralized in a certain form, resulting in an increase in the microhardness of the caries area and a decrease in porosity. The histomorphology shows that the surface layer and dark zone are widened, the area of caries is reduced, and the negative birefringence of the glazed surface is enhanced under the polarized light microscope. In the caries lesion area, the positive birefringence tends to the negative birefringence, and the microscopic X-ray shows an increase in density. In addition, remineralization not only refers to the deposition of
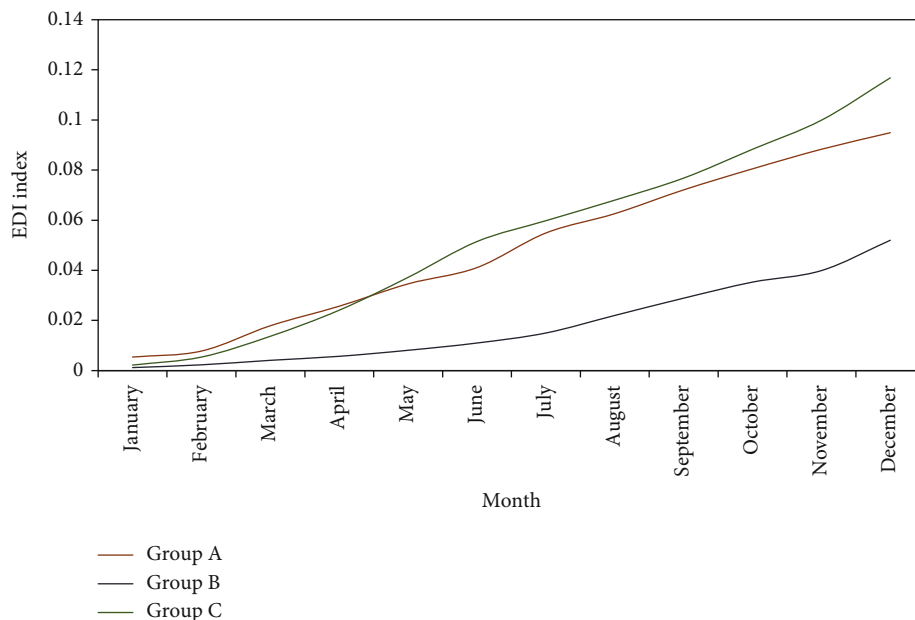
FIGURE 9: The average of the three groups of EDI indexes A, B, and C.

TABLE 5: Comparison of the numbers and proportions of the two groups of Streptococcus mutans and Actinomycetes.

| Bacteria | Number | | The proportion | |
|---|---|---|---|---|
| | Demineralization group | Undemineralized group | Demineralization group | Undemineralized group |
| Streptococcus mutans | $11.13 \pm 0.72$ | $10.63 \pm 0.91$ | $1.20 \pm 1.07$ | $0.44 \pm 0.48$ |
| Actinomycetes | $12.08 \pm 0.24$ | $12.11 \pm 0.57$ | $6.50 \pm 4.57$ | $8.59 \pm 10.51$ |

minerals in the oral cavity on the surface of the tooth and the diseased part under normal conditions but also can occur during the formation of dental caries.

The anterior teeth of the same name are similar in shape, and the contact surfaces and methods of the left and right anterior teeth of the same name and the toothbrush are similar when individuals perform daily oral cleaning such as brushing their teeth. This may also be one of the reasons. In the same dental arch, there is a statistical difference in the pH of the labial surface of the teeth without the same name. In the maxillary arch, the pH of the labial surface of the canine teeth is higher than that of the central incisor ($P < 0.05$), and both are significantly higher than that of the lateral incisor ($P < 0.05$); this may be related to the position of the teeth in the oral cavity and the distance of the salivary gland opening. For example, the pH of the labial surface of the maxillary lateral incisor is lower than that of the canine. Plaque is easy to accumulate, especially after bonding and fixing the appliance, it affects its cleaning and makes the pH of the lip surface lower than the central incisor. There is no significant difference in pH between mandibular lateral incisors and central incisors. Therefore, the central incisors and lateral incisors of the mandibular incisors receive the washing and buffering effect of saliva resemblance. This is similar to the difference in enamel demineralization in fixed orthodontics.

Due to the low compliance of patients, topical fluoride regimens are usually difficult to work. Calcium and phosphate ions released from calcium phosphate biomaterials form ion reservoirs in dental plaques. The supersaturated calcium and phosphorus ion pool helps prevent demineralization and promote enamel remineralization. In traditional calcium phosphate materials, the diameter of calcium phosphate fillers is mostly about 55 microns, which leads to restrictions on the filler addition ratio and the release of calcium and phosphorus ions. The new type of amorphous calcium phosphate nanoparticles (NACP) has a diameter of about 110 nm. Because of its small particle size and large specific surface area, it has a high level of Ca and P ion release ability and the ability to promote tooth enamel remineralization. In addition, resin composites containing this type of NACP filler can "smartly" release high concentrations of calcium and phosphorus ions in an environment with a pH value close to 4 (cariogenic environment and enamel demineralization environment), and increase the local pH to above 5.5. Reduce the enamel demineralization rate, and after the pH rises above 5, the release of ions will be significantly reduced, preserving the effectiveness of the internal filler of the material.

The copolymer has a large difference in solubility between the hydrophilic and hydrophobic segments and can self-assemble into nanomicelles with a fairly narrow size

distribution and typical core-shell structure in water. Polyethylene glycol (PEG) is often used as the hydrophilic segment of polymer micelles, and the hydrophobic segment is polylactic acid (PLA), chitosan (CS), polycaprolactone (PLC), etc. The inner core can be loaded with poorly water-soluble drugs to increase the solubility of the drugs in aqueous solutions, while the hydrophilic outer shell can maintain the steric stability of the micelles. Polymer micelles can escape the nonspecific uptake of the reticuloendothelial system (RES) due to their small size distribution; the preparation methods of micelles are simple and diverse, and the conditions are mild; targeting molecules can be coupled on the surface of the micelles to enable the drug to achieve the target to deliver, thereby improving the efficacy of drugs. These advantages make polymer micelles have broad application prospects in the delivery of poorly soluble drugs.

## 5. Conclusions

Enamel demineralization of orthodontic teeth is a very serious problem, especially for patients with poor oral hygiene, and it is necessary to take active preventive measures as soon as possible. The self-etching bonding technology breaks through the traditional phosphoric acid etching and combines a variety of research results to reduce enamel damage and demineralization. It has special advantages in preventing enamel demineralization and is worthy of further research. The surface of the enamel after acid etching demineralization is rougher, and the porosity is greater, which is conducive to the penetration and fitting of the adhesive. The nanoactive filler contained in the adhesive is easier to combine with the demineralized enamel, thereby enhancing the hardness. Over time, the loss or increase of minerals ultimately determines whether WSL or even dental caries will advance, stabilize, or degenerate. Therefore, improving the ability of tooth enamel to resist demineralization and promoting its remineralization is an effective method to inhibit WSL and dental caries. In the experiment, the synthetic peptide at the C-terminus of enamel protein improved the directional connection of the nanoparticles and promoted the orderly transformation of the nanoparticles into enamel-like HAP crystals. Ordered particle arrangement may be a preparatory step before crystal formation and growth, which is in line with the concept of particle-attached crystallization (CPA) in the nonclassical mineralization theory. In this study, CMC and PA are used to simulate proteins related to biomineralization, and ACP is stabilized and arranged by forming CMC/ACP nanocomposites, and then, small particles are arranged in a queue and specifically bound to the enamel surface.

## Data Availability

Data sharing is not applicable to this article as no datasets were generated or analyzed during the current study.

## Conflicts of Interest

The authors declare that they have no conflicts of interest.

## References

[1] L. Jiang, Y. Li, Y. Shao et al., "Enhanced removal of humic acid from aqueous solution by novel stabilized nano-amorphous calcium phosphate: behaviors and mechanisms," *Applied Surface Science*, vol. 427, pp. 965–975, 2018.

[2] G. Feng, C. Qin, F. Sha, Y. Lyu, and X. Jiang, "Evaluation of inflammatory and calcification after implantation of bioabsorbable poly-L-lactic acid/amorphous calcium phosphate scaffolds in porcine coronary arteries," *Journal of Nanomaterials*, vol. 2021, Article ID 6652648, 8 pages, 2021.

[3] Y. Zhang, X. She, X. Gao, C. Shan, and B. Pan, "Unexpected favorable role of Ca~(2+) in phosphate removal by using nanosized ferric oxides confined in porous polystyrene beads," *Environmental Science & Technology*, vol. 53, no. 1, pp. 365–372, 2019.

[4] M. Mohamed, W. Refaat, and S. Morcos, "Effect of different fluoride releasing bonding agents in preventing of enamel demineralization around orthodontic brackets," *Egyptian Orthodontic Journal*, vol. 50, no. 12, pp. 13–34, 2020.

[5] S. Chakraborty, H. Kidiyoor, and A. K. Patil, "Effect of light-curable fluoride varnish and conventional topical fluoride varnish on prevention of enamel demineralization adjacent to orthodontic brackets: a comparative study," *The Journal of Indian Orthodontic Society*, vol. 54, no. 1, pp. 14–23, 2020.

[6] R. Reddy, R. Manne, G. C. Sekhar, S. Gupta, N. Shivaram, and K. R. Nandalur, "Evaluation of the efficacy of various topical fluorides on enamel demineralization adjacent to orthodontic brackets: an in vitro study," *The Journal of Contemporary Dental Practice*, vol. 20, no. 1, pp. 89–93, 2019.

[7] N. B. Ulusoy, A. A. Oba, and Z. C. Cehreli, "Effect of Er, Cr: YSGG laser on the prevention of primary and permanent teeth enamel demineralization: SEM and EDS evaluation," *Photomedicine and Laser Surgery*, vol. 38, no. 5, pp. 308–315, 2020.

[8] B. Panariello, A. Azabi, L. Mokeem et al., "The effects of charcoal dentifrices on Streptococcus mutans biofilm development and enamel demineralization," *American Journal of Dentistry*, vol. 33, no. 1, pp. 12–16, 2020.

[9] D. A. Krivtsova and E. E. Maslak, "Monitoring the results of enamel demineralization treatment with the caries infiltration method (according to laser fluorescence value)," *Pediatric Dentistry And Dental Profilaxis*, vol. 20, no. 1, pp. 37–41, 2020.

[10] D. H. Shivananda, W. Ansar, A. R. Dinsha et al., "Effectiveness of various dental varnishes in prevention of enamel demineralization around orthodontic brackets: an in vitro study," *The Journal of Contemporary Dental Practice*, vol. 21, no. 6, pp. 621–625, 2020.

[11] T. I. Vieira, A. K. Alexandria, J. Menezes et al., "Characterization and effect of nanocomplexed fluoride solutions on the inhibition of enamel demineralization created by a multispecies cariogenic biofilm model," *Clinical Oral Investigations*, vol. 24, no. 11, pp. 3947–3959, 2020.

[12] H. Mo, J. Kim, and S. Oh, "Comparison of prevention methods against enamel demineralization adjacent to orthodontic bracket using fluoride," *The Journal of the Korean Academy of Pedtatric Dentistry*, vol. 46, no. 3, pp. 293–300, 2019.

[13] M. L. Torres-Garcia, L. D. Llavore, A. Bungay, J. D. Sarol Jr., R. R. Pineda, and K. . Peñas, "Benzalkonium chloride in an orthodontic adhesive: its effect on rat enamel demineralization using color-based image analysis," *American Journal of Orthodontics & Dentofacial Orthopedics*, vol. 155, no. 1, pp. 88–97, 2019.

[14] L. T. Trevelin, J. Villanueva, C. A. Zamperini, M. T. Mathew, A. B. Matos, and A. K. Bedran-Russo, "Investigation of five α-hydroxy acids for enamel and dentin etching: demineralization depth, resin adhesion and dentin enzymatic activity," *Dental Materials*, vol. 35, no. 6, pp. 900–908, 2019.

[15] R. Swetha, S. Manipal, M. Rajmohan et al., "Demineralization of tooth enamel surface at different immersion times of sport drink and buffering effect of casein derivative against enamel erosion," *International Journal of Advanced Research*, vol. 8, no. 10, pp. 926–935, 2020.

[16] Y. Tang, Z. Chen, W. Feng, Y. Nong, C. Li, and J. Chen, "Combined effects of nano-silica and silica fume on the mechanical behavior of recycled aggregate concrete," *Nanotechnology Reviews*, vol. 10, no. 1, pp. 819–838, 2021.

[17] C. Xiyue, L. Min, Z. Mu et al., "Synergetic PtNP@Co3O4 hollow nanopolyhedrals as peroxidase-like nanozymes for the dual-channel homogeneous biosensing of prostate-specific antigen," *Analytical and Bioanalytical Chemistry*, vol. 414, no. 5, pp. 1921–1932, 2022.

[18] H. Jasim, D. Al-Dabagh, and M. Mahmood, "Effect of different bracket types on Streptococcus mutans count in orthodontic patients using fluoridated toothpaste," *Journal of Baghdad College of Dentistry*, vol. 32, no. 2, pp. 1–4, 2020.

[19] G. Bo, X. Ning, and X. Pengfei, "Shock wave induced Nano crystallization and its effect on mechanical properties," *Materials Letters*, vol. 237, no. 15, pp. 180–184, 2019.

[20] C. Puyén-Goicochea, J. Armas-Pérez, and M. Ortiz-Pizarro, "Effect of an educational intervention via WhatsApp on the oral hygiene orthodontic patients," *International Journal of Odontostomatology*, vol. 14, no. 4, pp. 575–580, 2020.

[21] M. F. N. Feres, O. Eissa, M. G. Roscoe, and T. El-Bialy, "Comparison of the condyle sagittal position of class I and class II division 2 in orthodontic patients," *The Journal of Contemporary Dental Practice*, vol. 21, no. 9, pp. 977–981, 2020.

[22] A. Kolemen, H. S. Hasan, and A. Azzawi, "Medline diastema of orthodontic patients - prevalence and etiology in Erbil population - a cross-sectional study," *International Journal of Research in Pharmaceutical Sciences*, vol. 11, no. 4, pp. 5997–6003, 2020.

[23] T. Finkelstein, Y. Shapira, A. M. Pavlidi et al., "Canine transposition–prevalence, distribution and treatment considerations among orthodontic patients," *The Journal of Clinical Pediatric Dentistry*, vol. 44, no. 4, pp. 268–273, 2020.

[24] O. Svystun, L. Schropp, A. Wenzel, J. M. D. C. Silva, M. H. Pedersen, and R. Spin-Neto, "Prevalence and severity of image-stitching artifacts in charge-coupled device–based cephalograms of orthodontic patients," *Oral Surgery, Oral Medicine, Oral Pathology and Oral Radiology*, vol. 129, no. 2, pp. 158–164, 2020.

[25] J. V. Ashley, R. S. Ireland, and D. J. Plunkett, "Does the All Wales Universal Orthodontic Referral Form enable accurate triage of new NHS orthodontic patients? A service evaluation," *British Dental Journal*, vol. 228, no. 5, pp. 355–360, 2020.

[26] B. S. B. Bahar, S. R. Alkhalidy, E. G. Kaklamanos, and A. E. Athanasiou, "Do orthodontic patients develop more gingival recession in anterior teeth compared to untreated individuals? A systematic review of controlled studies-ScienceDirect," *International Orthodontics*, vol. 18, no. 1, pp. 1–9, 2020.